

On reaction processes with saturating diffusion

Alexander Kurganov¹ and Philip Rosenau²

¹ Department of Mathematics, Tulane University, New Orleans, LA 70118, USA

² School of Mathematical Sciences, Tel-Aviv University, Tel-Aviv 69978, Israel

E-mail: kurganov@math.tulane.edu and rosenau@post.tau.ac.il

Received 29 March 2005, in final form 30 August 2005

Published 8 November 2005

Online at stacks.iop.org/Non/19/171

Recommended by L Ryzhik

Abstract

Reaction–diffusion processes occur in a wide variety of physical and biological settings. When the saturation of the diffusion flux, as is to be expected of a physical process at high gradients, is incorporated into these processes, it may cause a fundamental change in the ensuing morphology, since now not only discontinuous equilibria become admissible, *but they may emerge instead of travelling waves* (TWs). A class of such processes, modelled by the equation $u_t = [Q(u_x)]_x - \beta^2 f(u)$, is studied both analytically and numerically. The diffusion flux Q is assumed to be a bounded increasing function with a sufficiently fast saturation rate, $\beta > 0$ is a constant, and a typical $f(u) \equiv f(u; \alpha_1, \dots, \alpha_N)$ with $f(0; \cdot) = f(1; \cdot) = f(\alpha_i; \cdot) = 0$, $i = 1, \dots, N$ has a sequence of control parameters $\alpha_i \in (0, 1)$. We show that the conventional equilibria kinks connecting upstream with downstream states may, when the parameter β exceeds a critical threshold, have a discontinuous part. Moreover, while in the conventional case of a linear Q when the total reaction is nonzero ($\int_0^1 f(u) du \neq 0$) TWs form, a bounded Q enables discontinuous equilibria, provided β is sufficiently large. Remarkably, when the number of possible constant equilibria is greater than two, the pattern may admit more than one discontinuity. Uniqueness of such states depends on the class of initial data assumed. We also numerically demonstrate that these new equilibria are robust and are (strong) attractors for a wide class of initial data.

Mathematics Subject Classification: 35K57, 35K65, 35B65

(Some figures in this article are in colour only in the electronic version)

1. Introduction

Since the first works on reaction–diffusion processes appeared over some sixty years ago the subject has seen growth in terms of physical, chemical and biological processes being found

to be described by such systems and the variety of mathematical tools developed to study such systems. The present work addresses another aspect relevant to such systems which, at least in the present context, appears to be new; namely in realistic diffusion processes, characterized in the small gradients limit by linear gradient-flux relations, the flux response to an increase of gradients has to slow down and ultimately approach saturation at large gradients. As we shall see, paying due respect to systems behaviour at large gradients introduces a deep impact on the morphology of the ensuing patterns, most notable of which is the possibility of piecewise continuous equilibrium states precluded by the conventional diffusion. The present work continues our previous studies of the impact of diffusion saturation [3, 4, 7, 9, 13, 14] on diffusive and convective–diffusive processes. The model equation to be studied is

$$u_t = [Q(u_x)]_x - \beta^2 f(u), \quad (1.1)$$

where β is a positive constant, $f(u)$ is a smooth function and $Q(s)$ is a *bounded increasing* smooth function satisfying $Q(0) = 0$ and $Q'(s) > 0, \forall s$. We also assume that the integral $\int_0^\infty s Q'(s) ds$ is finite or, equivalently, that the saturation rate is sufficiently fast, that is, for large $|s|$:

$$Q'(s) \sim K_\infty |s|^{-\gamma}, \quad \gamma > 2, \quad K_\infty > 0. \quad (1.2)$$

A particular form of Q to be used, unless otherwise mentioned, is

$$Q(s) = \frac{s}{\sqrt{1+s^2}}, \quad (1.3)$$

for which $\gamma = 3$ and $K_\infty = 1$. The rationale behind this particular choice of Q will be given shortly.

As specific examples of the reaction functions we will take $f(u)$ to be either of the Allen–Cahn type:

$$f(u) = f_3(u; \alpha) := u(u - \alpha)(u - 1), \quad 0 < \alpha < 1 \quad (1.4)$$

or a quintic reaction function

$$f(u) = f_5(u; \alpha_1, \alpha_2, \alpha_3) := u(u - \alpha_1)(u - \alpha_2)(u - \alpha_3)(u - 1), \quad 0 < \alpha_1 < \alpha_2 < \alpha_3 < 1. \quad (1.5)$$

The quintic case was chosen as the simplest example of a reaction with more than two stable equilibria. As we will see, it affords a much richer morphology than possible in the cubic case. All in all, the two cases suffice to show ‘unity through diversity’: details change with f , but all cases share a unifying theme—saturating diffusion may induce piecewise continuous equilibria which are otherwise precluded. Obviously, if the saturation is disregarded, the flux is a linear function, $Q(s) = Ds$, and equation (1.1) reduces to the standard reaction–diffusion equation:

$$u_t = Du_{xx} - \beta^2 f(u). \quad (1.6)$$

Though the boundedness of the flux function Q is a fundamental property of real physical systems, this feature is almost always lost in the weakly nonlinear, small gradients expansions, underlying the derivation of most, if not all, continuum models. The synthesized form of the saturation flux used here and in our earlier works [11, 13] is in a sense a Padé approximant, which smoothly connects the universal features of the flux function at the very small and very large gradients. Due to insufficient knowledge of the flux function valid across the whole range of wavelengths, there is some arbitrariness in the choice of the saturating flux function Q . Yet, our past studies repeatedly revealed that, insofar as Q is monotone in gradients and saturates *above a certain rate*, the particulars of the flux function are to a large extent of secondary importance.

Our model equation can also be seen as a flow described by

$$u_t = -\frac{\delta}{\delta u} E(u, u_x),$$

where

$$E(u, u_x) = \int_X [P(u_x) + \beta^2 F(u)] dx \quad (1.7)$$

is the free energy functional with $P'(s) = Q(s)$ and $F'(u) = f(u)$. The function P that corresponds to the choice of Q in (1.3) is

$$P(s) = \sqrt{1 + s^2}. \quad (1.8)$$

To comprehend how saturating diffusion shapes the emerging patterns, we first briefly restate its impact on the purely diffusive process, described by

$$u_t = [Q(u_x)]_x, \quad (1.9)$$

which has the remarkable property of *delaying the resolution of discontinuities* [2, 14]. Thus if the initial datum, $u_0(x) := u(x, 0)$, is discontinuous at a point x_0 and if the saturation rate condition (1.2) is satisfied, then there exists a finite time $T > 0$ such that the solution $u(x, t)$ remains discontinuous until then and continuous thereafter. Note that though saturation of the flux is an essential condition in delaying the resolution of discontinuities, it is not a sufficient condition, and an appropriate saturation rate is needed to sustain discontinuities. The saturation in such a case will be referred to as *a strong saturation*. Otherwise, the discontinuity disappears immediately [2, 14], and the saturation is considered to be *weak*.

If a nonlinear convection term appends equation (1.9)

$$u_t + \varphi(u)_x = [Q(u_x)]_x, \quad (1.10)$$

the situation changes drastically [7, 9, 12]. Unlike diffusion that describes relaxation, the nonlinear convection stimulates the breakdown of the solutions: while small amplitude kinks remain smooth, large amplitude kinks have embedded *subshocks*. The formation of discontinuities is a result of an imbalance between the inertial forces, which can be made arbitrarily large, and the limited response, which saturating diffusion can provide. Thus, when the applied force exceeds a critical threshold, discontinuities form and may persist indefinitely. In [9, 12], it was also demonstrated that both continuous and discontinuous travelling waves (TWs) are *strong attractors for a wide class of appropriate initial data*. For comprehensive analysis of equation (1.10), see [7, 9, 15]. Note that in such a process, weak and strong saturations have a similar impact and the qualitative behaviour of solutions is independent of the saturation rate.

Turning to the problem at hand, it is thus to be expected that embedding a strongly saturating diffusion mechanism into the reaction–diffusion process, (1.1), may lead to the emergence of discontinuities if certain supercritical conditions are satisfied. *This, indeed, is the main theme of the present work: we unfold a robust equilibrium mode embedded with a subshock, in a regime where conventional theory predicts smooth TWs or an equilibrium*. Since in the multi-equilibrium set-up, as represented by f_5 , the balanced case may instead of equilibrium induce a number of TWs (two in the quintic case), a saturating diffusion may replace TWs with an equilibrium containing jumps.

The plausibility of such jumps can be easily understood via the free energy functional (1.7). In the conventional case wherein P is quadratic in gradients, any jump implies an infinite energy and therefore such states are precluded. On the other hand, P s like the one in (1.8) predict a finite energy across a sharp interface and are thus admissible. Insofar as the free energy is concerned all that matters is whether the energy of the inhomogeneous phase can remain finite

across a sharp interface [11, 12]. From this point of view, it is easy to understand some recent related works where (1) the diffusion was modelled by a global convolution operator [1, 6, 16], which, having a bounded energy across a finite jump discontinuity, supports such states or (2) the diffusion operator was replaced with a centred difference on a lattice [5, 8]. In the latter discrete case, the chain's intersite energy is not only finite but slows down at a rate which enables the persistence of discontinuous states.

This paper is organized as follows. In section 2, we discuss TWs and steady-state kinks for equation (1.1) with the reaction term f_3 given by (1.4). We distinguish between the cases of balanced (section 2.1), where conventional kinks, at least in principle, are possible, and unbalanced (section 2.2) reaction processes, where the emerging stationary kinks *have no classical counterpart*. In section 3, we extend our studies to the quintic reaction f_5 given by (1.5). The quintic case appears to be the simplest set-up with multiple stable equilibria, and thus the solution may consist of two waves or, when saturation enters, equilibria with two jumps or one jump and one TW. A two-dimensional (2D) extension of the model equation (1.1) is briefly discussed in section 4.

2. Travelling and stationary patterns

Steadily TWs are solutions of the form

$$U(z) = u(x - \lambda t), \quad z := x - \lambda t, \quad \lambda = \text{const}, \quad (2.1)$$

that satisfy the following boundary conditions at $z = \pm\infty$:

$$\lim_{z \rightarrow -\infty} U(z) = U_L, \quad \lim_{z \rightarrow \infty} U(z) = U_R, \quad U_L = \text{const}, \quad U_R = \text{const}, \quad U_L \neq U_R.$$

Obviously, one should assume that $f(U_R) = f(U_L) = 0$. Substituting (2.1) into (1.1) results in the following second-order ODE:

$$-\lambda U' = [Q(U')] - \beta^2 f(U). \quad (2.2)$$

Multiplying (2.2) by U' and integrating by parts gives the velocity of the TW:

$$\lambda = \beta^2 \frac{\int_{U_L}^{U_R} f(u) du}{\int_{-\infty}^{\infty} (U')^2 dz} = \beta^2 \frac{F(U_R) - F(U_L)}{\int_{-\infty}^{\infty} (U')^2 dz}, \quad (2.3)$$

where $F' = f$. It is clear now that similarly to the linear diffusion case (1.6), the velocity of the TW vanishes if *the reaction function is balanced, that is, if* $\int_{U_L}^{U_R} f(u) du = F(U_R) - F(U_L) = 0$. This has a simple interpretation: let u be a temperature; then the balanced case means that the total heat production of sources is exactly balanced by the sinks. It is thus natural that in the unbalanced case, the net excess will induce a wave which tries to restore a balance. A TW with $\lambda \neq 0$ is possible provided, of course, $\int_{-\infty}^{\infty} (U')^2 dz$ is finite. In the classical case, wherein all solutions are smooth this would be the end of the argument, but since saturating diffusion supports, at least in principle, discontinuous solutions, a new possibility arises: *a steady unbalanced state*. We will demonstrate in section 2.2 that, in fact, this is a possibility. Due to the jump in U , only parts of the reaction function $f(U)$ are sampled in such a way that the heat sources are exactly balanced by the sinks. Thus the jump restores the energetic balance in the system. Notably, from (2.3) we deduce one more thing, *a TW cannot be discontinuous*. Therefore, since the main impact of saturation is to be experienced by steady states, our efforts will focus on understanding these phenomena.

2.1. Steady states. Part I: the balanced case

Steady-state solutions of (1.1) satisfy equation (2.2) with $\lambda = 0$, $z = x$ and $U = U(x)$:

$$[Q(U')] = \beta^2 f(U). \quad (2.4)$$

Multiplying this equation by U' , integrating from $-\infty$ to x and taking into account the fact that in the balanced case $F(U_R) - F(U_L) = 0$ results in the first-order ODE:

$$\tilde{Q}(U') = \beta^2 [F(U) - F(U_L)], \quad \tilde{Q}'(s) \equiv sQ'(s), \quad \tilde{Q}(0) = 0, \quad (2.5)$$

which can be easily analysed.

Notice that the saturation rate condition (1.2) guarantees that the function \tilde{Q} is bounded. Therefore, a solution of (2.5) has to be discontinuous if β^2 is chosen sufficiently large so that for some U s the values of $\beta^2[F(U) - F(U_L)]$ are out of the range of \tilde{Q} . For that matter insofar as Q is bounded and monotone (this has to do with the stability of these states) and satisfies (1.2), its explicit form is irrelevant.

We also note that if the saturation is weak, that is, if the condition (1.2) is not satisfied, the function \tilde{Q} is unbounded and hence there is no imbalance between the left-hand sides (LHS) and the right-hand side (RHS) of equation (2.5) and no discontinuous steady states are possible. Since the weak saturation case is similar to the case of linear Q , in what follows we will only consider strong saturation.

2.1.1. Continuous and discontinuous steady states. As a specific example, we consider Q given by (1.3), and $f = f_3$ as given by (1.4) with $\alpha = 1/2$, which corresponds to the balanced case. In this example,

$$\tilde{Q}(U') = 1 - \frac{1}{\sqrt{1 + (U')^2}}, \quad F_3(U) = \frac{U^2(1 - U)^2}{4}. \quad (2.6)$$

Let us now take, for instance, $U_L = 1$ and $U_R = 0$. Equation (2.5) then reduces to the equation

$$\frac{1}{\sqrt{1 + (U')^2}} = 1 - \frac{\beta^2}{4} U^2(1 - U)^2, \quad (2.7)$$

which will have a unique smooth solution only for $\beta < 8$, for which the RHS of (2.7) is positive for all $U \in [0, 1]$. If $\beta = 8$ (this is the critical value), then the solution is still continuous, but at the point where $U = 1/2$ its derivative will be infinite. Finally, in the supercritical case wherein $\beta > 8$, the solution of (2.7) is a weak solution consisting of two smooth pieces, connected through a subshock. Such a solution is properly defined in the sense of distributions only if both the left- and right-sided values of U' at the subshock are equal to $-\infty$ and the corresponding left(right)-sided values of U are $0.5(1 \pm \sqrt{1 - 8/\beta})$. The size of the jump is thus equal to $\sqrt{1 - 8/\beta}$. The sub and the supercritical cases are illustrated in figure 1.

Remark. We reiterate: though in the considered example a concrete saturated form was used, the conclusions are independent of the specifics of the particular saturated flux function Q . In fact, assume that Q is monotone, its saturation rate is given by (1.2), and \tilde{Q} is bounded by 1 (the latter can always be achieved by a proper rescaling); then most of the obtained results regarding the continuous and discontinuous steady states would still hold.

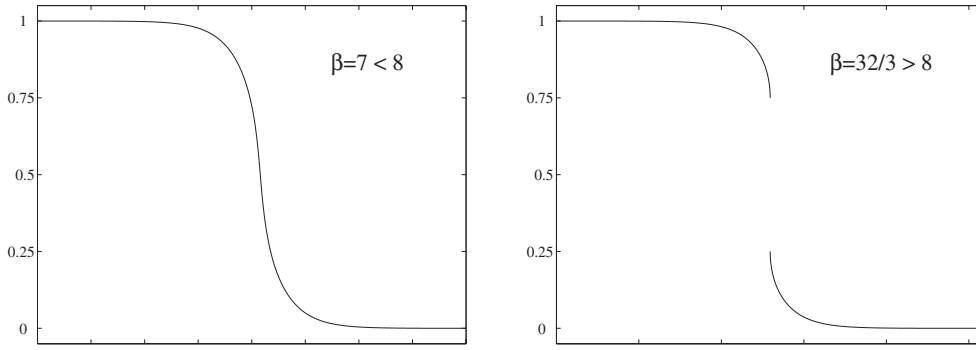


Figure 1. Steady-state solutions of equations (1.1), (1.3) and (1.4) for a subcritical $\beta = 7 < 8$ (left) and a supercritical $\beta = 32/3 > 8$ (right).

2.2. Steady states. Part II: the unbalanced case

This section is devoted to steady-state solutions of equation (1.1) in the unbalanced case, in which $F(U_R) - F(U_L) \neq 0$. As follows from (2.3), such solutions cannot be smooth since the integral $\int_{-\infty}^{\infty} (U')^2 dx$ must diverge. This obviously can happen if the solutions have a subshock and ‘square-root-type’ singularities on both sides of the subshock.

We now construct such discontinuous steady states. As noted in the previous case, though the actual calculations are done with a specific form of Q , most of the results are pretty much independent of the choice of Q insofar as Q is a bounded increasing function that saturates at a proper rate. It is the choice of f which mostly affects the resulting pattern. Without loss of generality, we also assume that the subshock is located at $x = 0$, and we integrate equation (2.4) on the intervals $(-\infty, 0)$ and $(0, \infty)$ separately. The resulting solution will then consist of two pieces: $U_-(x)$ and $U_+(x)$. The first function, $U_-(x)$, must satisfy the equation

$$\tilde{Q}(U'_-) = \beta^2[F(U_-) - F(U_L)], \quad x \in (-\infty, 0), \quad (2.8)$$

while the second function, $U_+(x)$, should be a solution of

$$\tilde{Q}(U'_+) = \beta^2[F(U_+) - F(U_R)], \quad x \in (0, \infty). \quad (2.9)$$

The two pieces are to be connected through the subshock and they both must have an infinite derivative at $x = 0$, namely U_- and U_+ should satisfy

$$\lim_{x \rightarrow 0^-} U'_-(x) = \lim_{x \rightarrow 0^+} U'_+(x) = -\infty. \quad (2.10)$$

Remark. Condition (2.10) guarantees that the speed of the subshock vanishes, and the constructed solution will indeed be steady. To verify this, we recall that the subshock speed, s , can be computed from the Rankine–Hugoniot condition, which implies

$$\begin{aligned} s &= \frac{[Q(U')]}{[U]} = \frac{\lim_{x \rightarrow 0^+} Q(U'_+(x)) - \lim_{x \rightarrow 0^-} Q(U'_-(x))}{U_+(0+) - U_-(0-)} \\ &= \frac{\lim_{p \rightarrow -\infty} Q(p) - \lim_{p \rightarrow -\infty} Q(p)}{U_+(0+) - U_-(0-)} = 0. \end{aligned}$$

2.2.1. *Emergence of discontinuous steady states.* We now consider a particular example of Q and $f = f_3$ given by (1.3) and (1.4), respectively. We also take $U_L = 1$ and $U_R = 0$. Then,

$$F_\alpha(U) := F(U) = U^2 \left(\frac{1}{4}U^2 - \frac{1+\alpha}{3}U + \frac{\alpha}{2} \right),$$

and equations (2.8) and (2.9) become

$$1 - \frac{1}{\sqrt{1+(U'_-)^2}} = \beta^2[F_\alpha(U_-) - F_\alpha(U_L)], \quad x < 0, \quad (2.11)$$

and

$$1 - \frac{1}{\sqrt{1+(U'_+)^2}} = \beta^2[F_\alpha(U_+) - F_\alpha(U_R)], \quad x > 0, \quad (2.12)$$

where, in the present case, $F_\alpha(U_L = 1) = (2\alpha - 1)/12$ and $F_\alpha(U_R = 0) = 0$, respectively. The boundary conditions (2.10) will then be satisfied if

$$F_\alpha(U_-(0)) = \frac{1}{\beta^2} + \frac{2\alpha - 1}{12}, \quad (2.13)$$

$$F_\alpha(U_+(0)) = \frac{1}{\beta^2}. \quad (2.14)$$

Since $1 > U_-(0) \geq U_+(0) > 0$ and since $\max_{u \in [0,1]} F_\alpha(u) = F_\alpha(\alpha)$, the range of the LHS of both (2.13) and (2.14) is $[0, F_\alpha(\alpha)] \equiv [0, \alpha^3(2 - \alpha)/12]$. Therefore, the solutions of the problems (2.11), (2.13) and (2.12), (2.14) will exist only if β is sufficiently large. We have two cases to consider.

Case 1: If $\alpha > 1/2$, the solution of (2.11)–(2.14) will exist provided

$$\frac{2 - \alpha}{12}\alpha^3 \geq \frac{1}{\beta^2} + \frac{2\alpha - 1}{12} \iff \beta^2 \geq \frac{12}{(1 + \alpha)(1 - \alpha)^3}. \quad (2.15)$$

Case 2: If $\alpha < 1/2$, the solution of (2.11)–(2.14) will exist provided

$$\frac{2 - \alpha}{12}\alpha^3 \geq \frac{1}{\beta^2} \iff \beta^2 \geq \frac{12}{(2 - \alpha)\alpha^3}. \quad (2.16)$$

Remark. Note that the balanced case ($\alpha = 1/2$) can obviously be included either in case 1 or case 2.

The conditions (2.15) and (2.16) can be written in a more compact form by introducing a parameter $\varepsilon = 2\alpha - 1$, $\varepsilon \in [-1, 1]$, so that we conclude that a discontinuous steady state exists only if

$$\beta^2 > \beta_*^2 := \frac{64}{(1 + |\varepsilon|/3)(1 - |\varepsilon|)^3}. \quad (2.17)$$

Otherwise, a solution of (2.4) will not exist, and the resulting solution of (2.2) will be a smooth TW that propagates with a nonzero speed λ . According to (2.3), its sign, and thus the direction of propagation, is determined by the sign of $F_\alpha(U_R) - F_\alpha(U_L)$, which is negative in case 1 and positive in case 2.

We are now ready to describe the morphology of the different flows. The full story is described in figures 2–5. The bifurcation diagram in figure 2 displays the parametric domain of the equilibria. Clearly, for a given ε , as long as $\beta > \beta_*$ (the supercritical case) the only possible solution of form (2.1) is a discontinuous steady state. As β decreases, the resulting

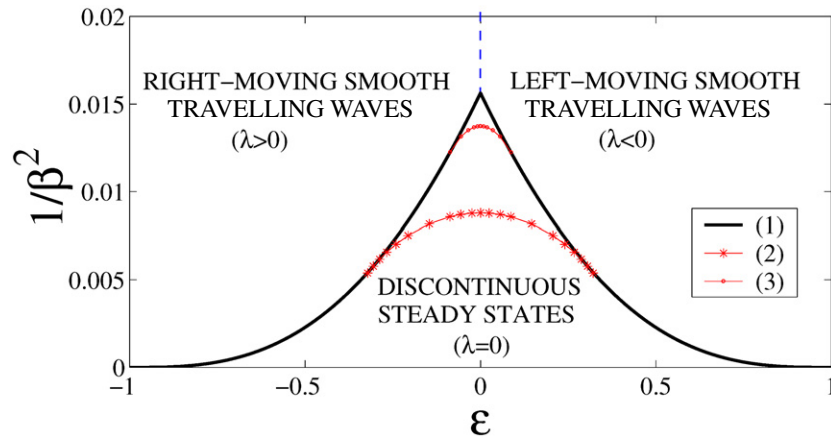


Figure 2. Curve (1) is the bifurcation curve in the $(\varepsilon, 1/\beta^2)$ -plane, $\varepsilon = 2\alpha - 1$, describing the different types of solutions of (2.2), (1.3) and (1.4). Within the ‘triangular’ domain the solution is a stationary piecewise continuous kink. Curves (2) and (3) describe equilibria with the same jump size, $1/2$ and $1/4$, respectively. The classical equilibria reside on the (---) vertical line which ends at the tip of the bifurcation curve. In the outer domain, except for the $\varepsilon = 0$ ($\alpha = 1/2$) line, waves travel either to the right (a heating wave) or to the left (a cooling wave).

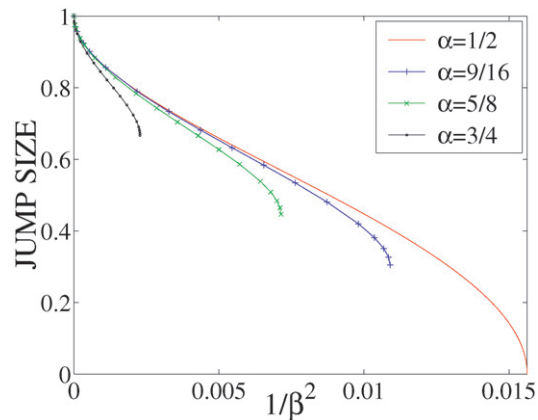


Figure 3. Jump size as a function of $1/\beta^2$ for different α s. $\alpha = 1/2$ represents the balanced case, with zero jump at the tip of the bifurcation curve and the maximal jump of size 1 at the bottom of the bifurcation ‘triangle’, where all other curves have a maximal jump of the same size as well. Their minimal jumps are obtained when the appropriate $\varepsilon = \text{const}$ line intersects with the bifurcation curve in figure 2.

jump becomes smaller and once $\beta < \beta_*$ (the subcritical case) then instead of a discontinuous steady state one obtains a smooth wave travelling with a nonzero speed λ . Obviously, the jump size is maximal at the bottom of the bifurcation ‘triangle’, that is, when $\beta \rightarrow \infty$. When ε is fixed (or, equivalently, α is fixed) and β decreases, the size of the jump decreases as well, as one can see in figure 3. The minimal jump is obtained at the upper boundary of the bifurcation ‘triangle’. Note that only in the balanced case ($\alpha = 1/2$) the size of the jump gradually decreases to 0.

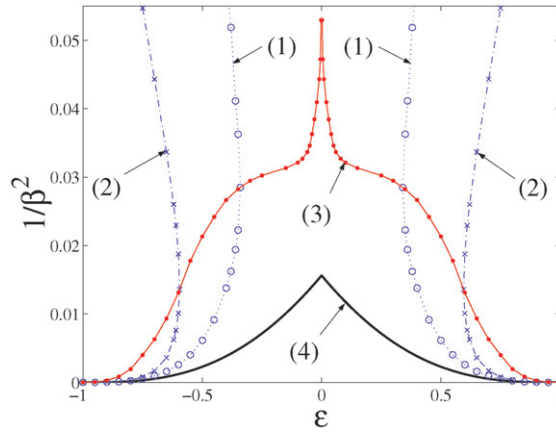


Figure 4. Landscape of TWs for a cubic reaction (2.2), (1.3) and (1.4) in the $(\varepsilon, 1/\beta^2)$ -plane, $\varepsilon = 2\alpha - 1$. (1) and (2) are the iso-speed curves with the corresponding TW speeds 1 and 2; (3) represents a ‘maximal speed’ KH-curve as given by the extremal points in figure 5; (4) is the bifurcation curve (see figure 2). In the area between the KH and the bifurcation curves, the saturation has an important impact on the dynamics of the TWs.

Figure 4 tells the story of the domain outside the bifurcation ‘triangle’. The most notable is the ‘kaiser helmet’ shape (KH) curve, which bounds from above a parameter domain wherein the TWs are heavily affected by the saturation. One way to follow that phenomenon is to start with a small β . One expects that for a given ε as the subcritical β increases, the resulting wave speed would increase as well. In the conventional case of a linear flux Q , this is an elementary conclusion from the scaling invariance under the change of variables

$$x \rightarrow kx, \quad t \rightarrow k^2t, \quad \beta \rightarrow \frac{\beta}{k}, \tag{2.18}$$

which implies that if the velocity λ corresponding to a specific β is known, then $k\lambda$ is the velocity corresponding to β/k . Thus, for a given ε , one has to determine the relevant speed once, and then all other speeds are obtained via scaling. In the case of a saturating diffusion flux, however, this simple scaling is lost, so that the $\lambda(\beta)$ relations have to be determined numerically, as shown in figure 5. The remarkable effect of saturation manifests itself with the KH-curve, which represents the maximal possible speed for a given ε . When β is further increased, the speed decreases until the TW disappears when one hits the bifurcation curve.

We now present a more detailed numerical study of a particular case of $\alpha = 3/4$, in which a steady state is discontinuous provided (2.15) is satisfied, that is if

$$\beta^2 > \beta_*^2 = \frac{3072}{7} \approx 20.9489^2.$$

Such a discontinuous steady-state solution for $\beta = 25$ is shown in figure 6.

We numerically demonstrate that the discontinuous steady states are attractors for a wide range of initial data. As an example, we take both the discontinuous,

$$u_0(x) = \begin{cases} 1, & \text{if } x < 0, \\ 0, & \text{if } x > 0, \end{cases} \tag{2.19}$$

and the smooth,

$$u_0(x) = \frac{1 - \tanh(2x)}{2}, \tag{2.20}$$

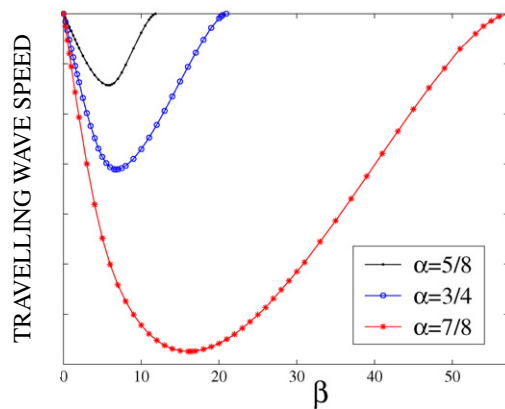


Figure 5. TW speed λ as a function of β for different α s. At the upper left corner the curves are roughly straight lines, which represent the conventional scaling (2.18). However, as β increases, the $\lambda(\beta)$ dependence becomes clearly nonlinear and the corresponding curves are almost concave—this represents a remarkable impact of saturation. The extremal points form the KH-curve in figure 4. Above the KH-curve, the left branch of the presented curves applies: though at a slower pace than the conventional process, the TW speed increases with β . Once the KH-curve is crossed, the right branch of the presented curves applies and the opposite holds: now an increase of β slows down the wave (and its profile steepens) until it hits the bifurcation curve, where TWs disappear and piecewise continuous equilibria emerge.

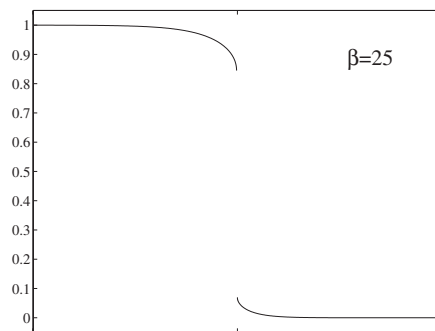


Figure 6. Discontinuous steady-state solution of (1.1)–(1.4) with $\beta = 25$.

initial data. The time evolution of these initial data for a supercritical $\beta = 25$ is shown in figure 7. One can clearly see that in both cases, the solution converges to a discontinuous steady state. For a subcritical $\beta = 15$, the solution first evolves into a TW and then propagates to the left (note that $F_\alpha(U_R) - F_\alpha(U_L) = -625/24 < 0$ here) with a constant speed, as demonstrated in figure 9. We compare these results with the corresponding ones in the case of the linear $Q(s) = s$, where no discontinuous solutions are possible, see figures 8 and 10.

Remarks.

(1) The *jump conditions* can be understood as follows. For $\alpha = 1/2$, the area under the graph of the positive part of f equals the area over its negative part: the heating part balances the cooling part, and the system can clearly be in equilibrium. When $\alpha \neq 1/2$, the net area bounded by f is nonzero, which implies an excess of heating or cooling. This results in a TW that propagates to re-balance the system. Saturated diffusion, which supports discontinuous states, may allow, however, another resolution of the dilemma: cut f at $u = U_+$ and $u = U_-$

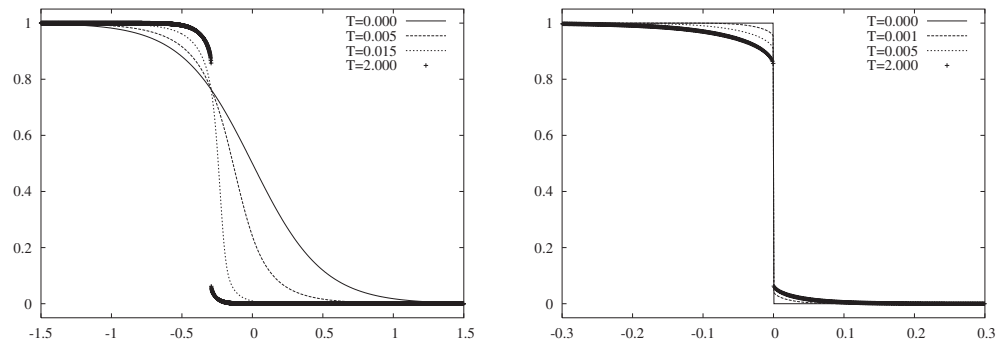


Figure 7. Nonlinear Q . Convergence to the discontinuous steady state for the smooth, (2.20), (left) and the discontinuous, (2.19), (right) initial data. $\beta = 25$.

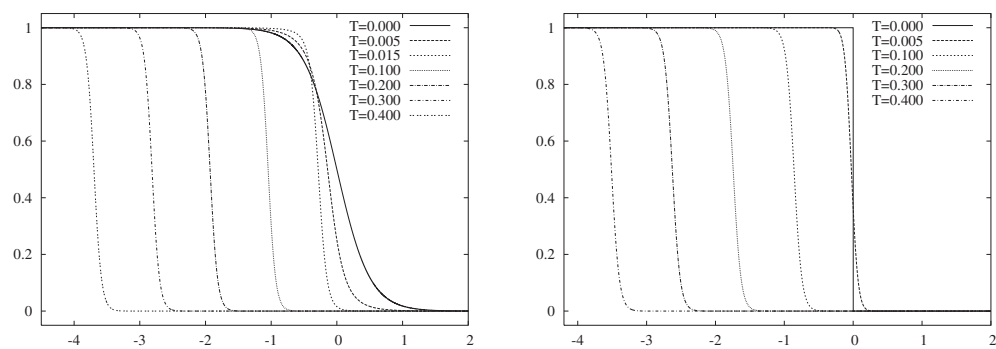


Figure 8. Linear Q . Convergence to the smooth TW for the smooth, (2.20), (left) and the discontinuous, (2.19), (right) initial data. $\beta = 25$.

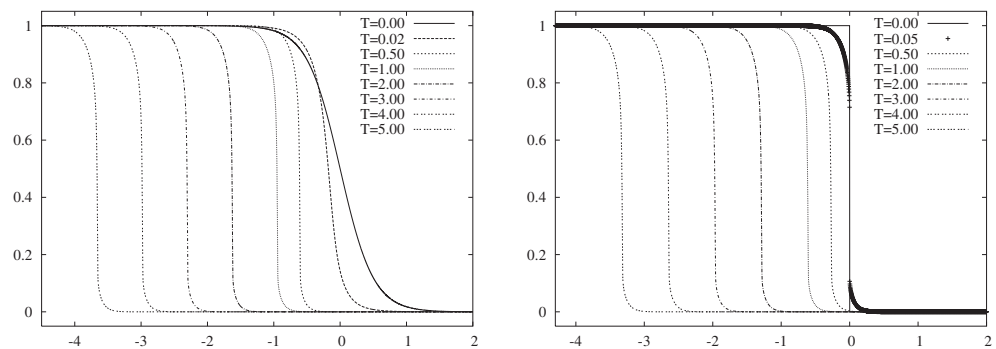


Figure 9. Nonlinear Q . Convergence to the smooth TW for the smooth, (2.20), (left) and the discontinuous, (2.19), (right) initial data. $\beta = 15$. In the second case, the saturation of diffusion causes an ‘inertial delay’: the front does not move until the initially imposed discontinuity diffuses away.

in such a way that the area under f in the $[0, U_+]$ interval balances the corresponding area in the $[U_-, 1]$ interval. The evaluation of the positions of the cuts is nothing more than the jump conditions we have just presented. Clearly, the jump separates a heating dominated zone from a cooling dominated zone.

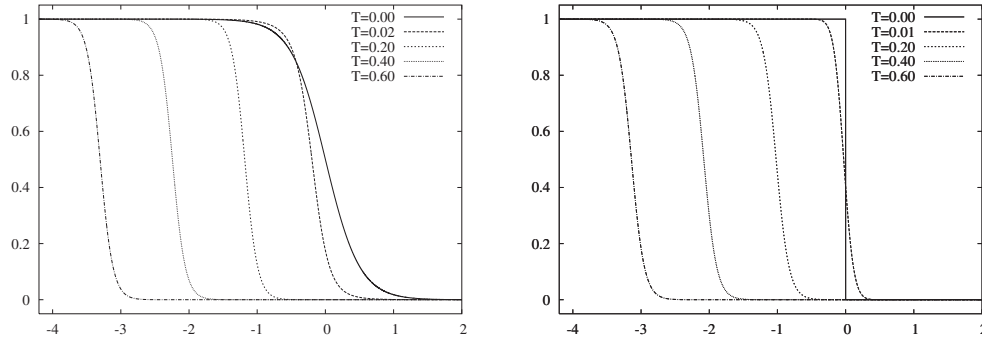


Figure 10. Linear Q . Convergence to the smooth TW for the smooth, (2.20), (left) and the discontinuous, (2.19), (right) initial data. $\beta = 15$.

(2) From the above discussion it also follows that when there is no parameter range that supports a global balance, discontinuous equilibria are also impossible. Indeed, since in a globally balanced system the ‘heating part’ of f must be exactly balanced by its cooling counterpart, f must change its sign *at least once* inside the $(0, 1)$ interval. Thus the cubic reaction (1.4) we use here as an example is, in fact, *the simplest generic f* , which, of course, excludes from consideration the quadratic f used in the Fisher/KPP equations. Also, note that a quartic polynomial $f(u) = f_4(u; \alpha_1, \alpha_2) := u(u - \alpha_1)(u - \alpha_2)(u - 1)$ with $0 < \alpha_1 < \alpha_2 < 1$ changes sign twice inside the $(0, 1)$ interval rendering the $u \equiv 1$ equilibrium unstable and has also to be excluded from consideration.

3. A quintic reaction

The next simplest f is given by a quintic polynomial (1.5):

$$f(u) = f_5(u; \alpha_1, \alpha_2, \alpha_3) := u(u - \alpha_1)(u - \alpha_2)(u - \alpha_3)(u - 1), \quad 0 < \alpha_1 < \alpha_2 < \alpha_3 < 1, \quad (3.1)$$

where α_1, α_2 and α_3 are control parameters.

A necessary condition for the total reaction function F to be in equilibrium ($F(0; \cdot) = F(1; \cdot) = 0$) imposes the following constraint on the α s:

$$\alpha_2 = \frac{3(\alpha_1 + \alpha_3) - 5\alpha_1\alpha_3 - 2}{5(\alpha_1 + \alpha_3) - 10\alpha_1\alpha_3 - 3}, \quad (3.2)$$

which implies that

$$F(u) = F(u; \alpha_1, \alpha_2, \alpha_3) = u^2(1 - u)^2 G(u), \quad G(u) := g_0 + g_1 u + \frac{u^2}{6},$$

where the parameters g_0 and g_1 are related to the α s via

$$2g_0 = \alpha_1\alpha_2\alpha_3, \quad 5g_1 = \frac{2}{3} - (\alpha_1 + \alpha_2 + \alpha_3).$$

Thus in the quintic case, for a given β there is a two parameter family of equilibria. We pause momentarily, since the quintic case is not as well known as its cubic sibling, to recall that in order to obtain a conventional equilibrium, the function G has to be free from real roots in $[0, 1]$. Otherwise a kink connecting 0 with 1 is impossible, and in this case, since $u \equiv \alpha_2$ is a stable equilibrium, the solution is made of two waves: a cooling wave that propagates to the left and ‘mediates’ between $1/2$ and 1 and a heating wave, which propagates to the

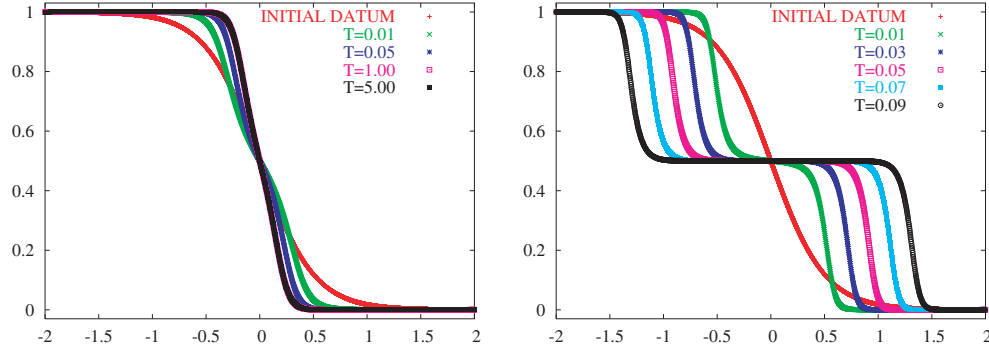


Figure 11. Linear $Q(s) = s$. Solutions of (1.1), (1.3) with $f = f_5$ and the initial datum (2.20). $\beta = 60, \alpha_1 = 1/4, \alpha_2 = 1/2, \alpha_3 = 3/4$ (left); $\beta = 100, \alpha_1 = 1/8, \alpha_2 = 1/2, \alpha_3 = 7/8$ (right).

right and ‘mediates’ between $1/2$ and 0 (this is an elementary consequence of the first integral of equation (2.4): $\frac{1}{2}(U')^2 - \beta^2 F(U; \alpha_1, \alpha_2, \alpha_3) = 0$). These two possibilities are clearly displayed in figure 11. In both cases, the resulting pattern is solely determined by the roots of G . Thus in a multi-equilibrium set-up, even when the system is globally balanced, locally it may be unbalanced which results in moving waves. This blurs to a large extent the distinction between balanced and unbalanced cases, which is vital in the cubic case.

We now begin our description of the impact of saturating diffusion on quintic morphology. We first summarize the main features:

- (1) As in the conventional case of a linear Q , the subcritical solution is either an equilibrium or two waves propagating in opposite directions.
- (2) Unlike the cubic case, a monotone solution may now contain either two jumps, one jump or no jumps at all.
- (3) For a symmetric F in the supercritical case, there are either two equal size jumps or only one transition connecting them.
- (4) When F is an asymmetric function, one can be in a subcritical regime with respect to one hump of F and in a supercritical regime with respect to the other hump. Consequently, we can have a solution consisting of one moving wave and one stationary shock, which brings to a halt a moving wave which will re-emerge if one returns to the subcritical regime.
- (5) Whenever two shocks emerge we can *a priori* calculate their strength (i.e. the size of each jump), but not the location of each of them which depends on the form of the particular initial data.

We start with the description of a two-jump solution. We seek a steady-state solution of equation (1.1), which is a solution of equation (2.5) on the following three intervals: $(-\infty, x_1)$, (x_1, x_2) and (x_2, ∞) , where x_1 and x_2 denote the corresponding subshock locations (let $x_1 < x_2$). Let $\lim_{x \rightarrow -\infty} U(x) = 1$ and $\lim_{x \rightarrow \infty} U(x) = 0$; then we expect to obtain three pieces of continuous solutions, $U_L(x)$, $U_M(x)$ and $U_R(x)$, each of which satisfies one of the following three ODEs:

$$\tilde{Q}(U'_L(x)) = \beta^2[F(U_L(x)) - F(1)], \quad x \in (-\infty, x_1), \quad (3.3)$$

$$\tilde{Q}(U'_M(x)) - \tilde{Q}(U'_M(x_m)) = \beta^2[F(U_M(x)) - F(\alpha_2)], \quad x \in (x_1, x_2), \quad (3.4)$$

$$\tilde{Q}(U'_R(x)) = \beta^2[F(U_R(x)) - F(0)], \quad x \in (x_2, \infty), \quad (3.5)$$

where x_m is a point where $U_M(x_m) = \alpha_2$.

Similarly to the case of a single subshock, discussed in section 2.2, the resulting three pieces are to be connected through two subshocks, and the corresponding jump conditions must be satisfied:

$$\lim_{x \rightarrow x_1^-} U'_L(x) = \lim_{x \rightarrow x_1^+} U'_M(x) = \lim_{x \rightarrow x_2^-} U'_M(x) = \lim_{x \rightarrow x_2^+} U'_R(x) = -\infty.$$

Using equations (3.3)–(3.5) and assuming that, as in the particular case (2.6), $\lim_{s \rightarrow -\infty} \tilde{Q}(s) = 1$, these jump conditions can be rewritten as follows:

$$1 = \beta^2 [F(U_L(x_1^-)) - F(1)], \quad (3.6)$$

$$1 - \tilde{Q}(U'_M(x_m)) = \beta^2 [F(U_M(x_1^+)) - F(\alpha_2)], \quad (3.7)$$

$$1 - \tilde{Q}(U'_M(x_m)) = \beta^2 [F(U_M(x_2^-)) - F(\alpha_2)], \quad (3.8)$$

$$1 = \beta^2 [F(U_R(x_2^+)) - F(0)]. \quad (3.9)$$

It is now clear that equations (3.6) and (3.9) uniquely determine the values of $U_L(x_1^-)$ and $U_R(x_2^+)$, respectively. The values of $U_M(x_1^+)$ and $U_M(x_2^-)$ will be then also uniquely determined from the balance requirements on the intervals $(0, \alpha_2)$ and $(\alpha_2, 1)$, namely from the following two relations:

$$\int_0^{U_R(x_2^+)} f(u) du = \int_{U_M(x_2^-)}^{\alpha_2} f(u) du, \quad \int_{\alpha_2}^{U_M(x_1^+)} f(u) du = \int_{U_L(x_1^-)}^1 f(u) du.$$

The size of the separation interval (x_1, x_2) , however, cannot be uniquely determined from the jump conditions (3.6)–(3.9). Indeed, (3.7) and (3.8) imply $F(U_M(x_1^+)) = F(U_M(x_2^-))$, but, in general, there are infinitely many pairs of (x_1, x_2) that satisfy this condition. It then follows from (3.7) (or (3.8)) that x_1 (and x_2) is determined by the value of $\tilde{Q}(U'_M(x_m))$, which, in turn, depends on the initial data, as is clearly indicated by our numerical experiments (see, e.g. figures 13 and 14). Quantifying this dependence analytically or numerically is still an open problem.

3.1. Stationary and nonstationary patterns: the balanced case

We consider separately symmetric and asymmetric F s. In the latter case, the two local maxima of F , attained at $u = \alpha_1$ and $u = \alpha_3$, are different and a richer morphology is possible.

3.1.1. A symmetric F . α_1 and α_3 are now at an equal distance from the corresponding edges of the domain, that is, $\alpha_1 + \alpha_3 = 1$. Then equation (3.2) imposes $\alpha_2 = 1/2$ and F attains its maximal value at $u = \alpha_1$ and $u = \alpha_3$:

$$\max_{u \in [0,1]} F(u) = F(\alpha_1) = F(\alpha_3) = \frac{1}{12}(\alpha_1 \alpha_3)^3 = \frac{1}{12}[\alpha_1(1 - \alpha_1)]^3.$$

Therefore, assuming the function \tilde{Q} is bounded by 1, we conclude from equation (2.5) that the critical β satisfies

$$\beta_*^{-2} = \frac{1}{12}[\alpha_1(1 - \alpha_1)]^3.$$

Since now $G(u) = \alpha_1(1 - \alpha_1)/4 + (u^2 - u)/6$, it will have two real roots in the interval $(0, 1)$ if $\alpha_1(1 - \alpha_1) < 1/6$, that is, if

$$0 < \alpha_1 < \alpha_{1*} := \frac{1 - \sqrt{1/3}}{2} \approx 0.211325.$$

The scenario now is as follows: for $\beta < \beta_*$ we obtain a classical solution which, like in the conventional case, is either a stationary kink or a TW, while in the supercritical case, the roots

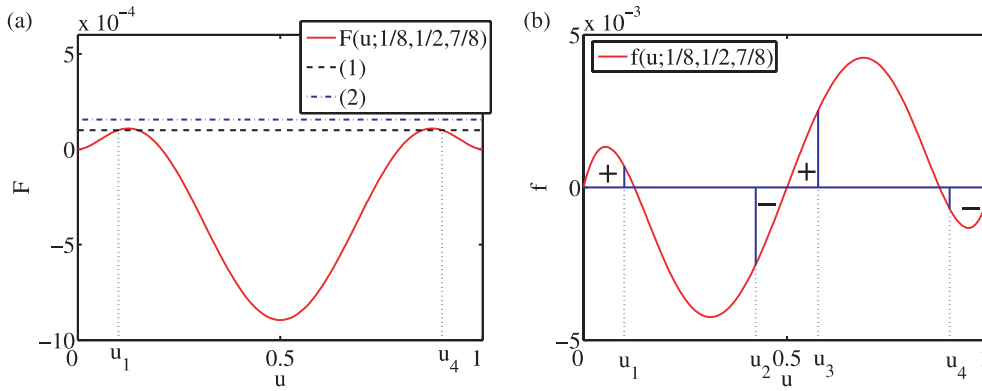


Figure 12. Graphs of $F(u; 1/8, 1/2, 7/8)$ (a) and $f(u; 1/8, 1/2, 7/8)$ (b). The horizontal lines of $1/\beta^2$ (1) ($\beta = 100$) and (2) ($\beta = 80$) represent the supercritical and the subcritical regimes, respectively. Here, $\beta_* \approx 95.7665$; $u_1 \approx 0.100022$, $u_2 \approx 0.423327$, $u_3 \approx 0.576674$ and $u_4 \approx 0.899978$.

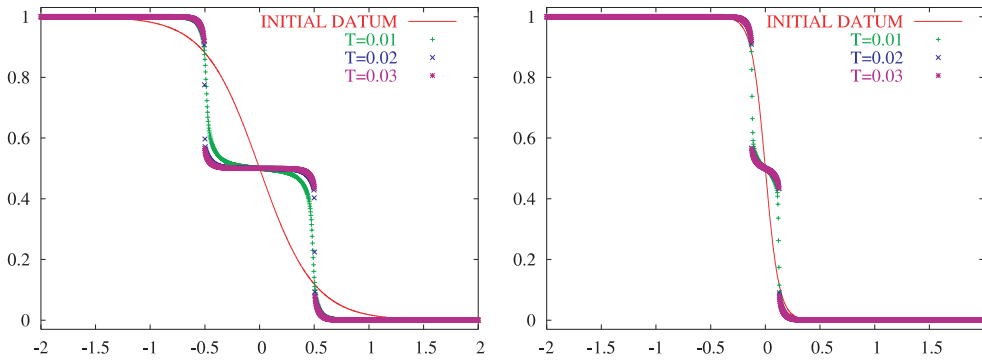


Figure 13. Solutions of (1.1), (1.3) with $f = f_5$ and the initial datum (3.10) with $\kappa = 2$ (left) and $\kappa = 8$ (right). A supercritical $\beta = 100$; $\alpha_1 = 1/8$, $\alpha_2 = 1/2$, $\alpha_3 = 7/8$.

of G do not play any role and a two-jump solution is always possible. Again, the distance between the two jumps is determined solely by the form of the initial conditions; in particular, it depends on the slope of the transition between the initial upstream and downstream states. If the initial transition is sharp, the resulting solution may consist of *one jump only*.

Next, we present a number of numerical studies, each exemplifying a different scenario.

Example 1 $\alpha_1 = 1/8 < \alpha_*$. We assume that $f = f_5$ is given by (3.1) with $\alpha_1 = 1/8$, $\alpha_2 = 1/2$ and $\alpha_3 = 7/8$. The resulting F is shown in figure 12(a). We numerically solve equation (1.1), (1.3) for two β s each representing a different regime, subject to the either smooth,

$$u_0(x) = \frac{1 - \tanh(\kappa x)}{2}, \quad \kappa = \text{Const} > 0, \quad (3.10)$$

or nonsmooth, (2.19), initial data. The computed solutions are shown in figures 13–15.

As one can clearly see in figures 13–15, in the supercritical case, a monotone (decreasing) solution may have either two jumps (from u_4 down to u_3 and from u_2 down to u_1) or one jump (from u_4 all the way down to u_1) only. Figure 12 is intended to clarify how the values of u_1 , u_2 , u_3 and u_4 can be determined. The symmetry of F implies symmetric (with respect

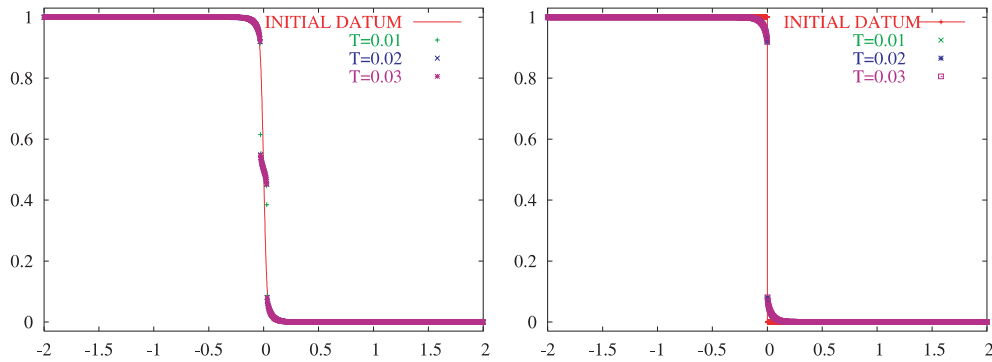


Figure 14. As in the previous figure, but with $\kappa = 32$ (left) and the initial datum (2.19) (right).

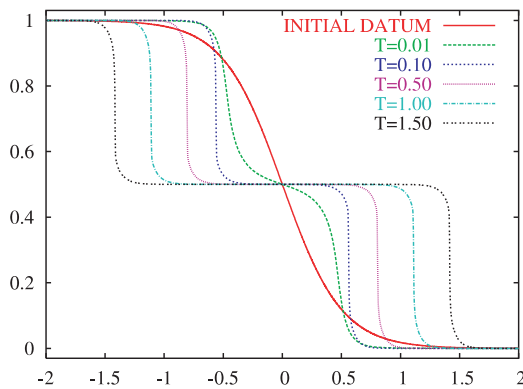


Figure 15. As in figure 13 (left), but with a subcritical $\beta = 80$.

to the edges) location of u_1 and u_4 and also of u_2 and u_3 . As is clear from figure 12(a), the intersection of the line $1/\beta^2$ and the graph of F determines the values of u_1 and u_4 , so that no solution with a continuous connection of u_4 with u_1 is possible. Figure 12(b) then shows how u_2 and u_3 can be determined: it is done by balancing the corresponding heating and cooling zones, namely by requiring

$$\int_0^{u_1} f(u) \, du = - \int_{u_2}^{1/2} f(u) \, du, \quad \int_{1/2}^{u_3} f(u) \, du = - \int_{u_4}^1 f(u) \, du.$$

The next example concerns the $\alpha_1 > \alpha_*$ case, in which F has no roots in $(0, 1)$: this is important in the subcritical regime, but is of no consequence in the supercritical one.

Example 2 $\alpha_1 = 1/4 > \alpha_*$. We now take $f = f_5$ with $\alpha_1 = 1/4$, $\alpha_2 = 1/2$ and $\alpha_3 = 3/4$. The function F is now non-negative (see figure 16). Again, we solve equation (1.1), (1.3) for a number of β s, subject to the either smooth, (2.20), or nonsmooth, (2.19), initial data. The results are shown in figure 17.

3.1.2. An asymmetric F . We still consider the balanced case, but now with asymmetrically distributed α s not symmetrically distributed. In this case, F has two different local maxima (a typical F is shown in figure 18), and thus instead of one critical value of $\beta = \beta_*$, we have

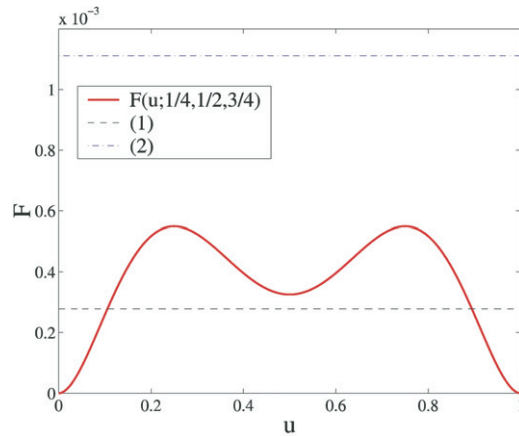


Figure 16. Graph of $F(u; 1/4, 1/2, 3/4)$. The horizontal lines of $1/\beta^2$ (1) ($\beta = 60$) and (2) ($\beta = 30$) represent the supercritical and the subcritical regimes, respectively. Here, $\beta_* \approx 42.6667$.

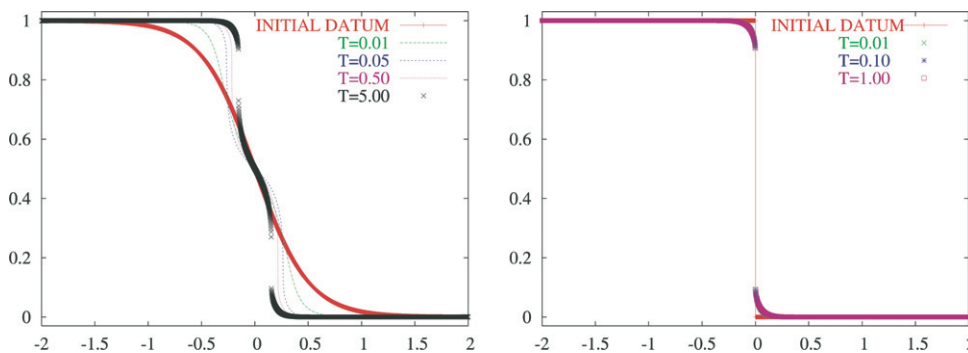


Figure 17. Solutions of (1.1), (1.3) with $f = f_5$ and the initial data (2.20) (left) and (2.19) (right). A supercritical $\beta = 60$; $\alpha_1 = 1/4, \alpha_2 = 1/2, \alpha_3 = 3/4$.

two critical β s: $\beta = \beta_{*,1}$ and $\beta = \beta_{*,2}$. Therefore, the following three scenarios are possible:

- (1) If $\beta < \beta_{*,1}$ (the subcritical case), a monotone solution will consist of two smooth waves propagating in opposite directions.
- (2) If $\beta_{*,1} < \beta < \beta_{*,2}$ (the intermediate case), the asymptotic form of a monotone solution will consist of one smooth moving wave and one steady shock.
- (3) If $\beta > \beta_{*,2}$ (the supercritical case), a monotone solution converges to a steady state with either two jumps or only one jump, depending on the sharpness of the initial datum.

Example 3 $\alpha_1 = 1/8, \alpha_2 = 5/14, \alpha_3 = 3/4$. The corresponding F is shown in figure 18. We numerically solve equation (1.1), (1.3) for different values of β and subject to the either smooth, (2.20), or nonsmooth, (2.19), initial data. The computed solutions are shown in figures 19–21.

Example 4 $\alpha_1 = 1/5, \alpha_2 = 2/5, \alpha_3 = 3/4$. In this example, we consider another asymmetric $f = f_5$ with $\alpha_1 = 1/5, \alpha_2 = 2/5$ and $\alpha_3 = 3/4$. The function F is now *non-negative* on the interval $[0, 1]$, see figure 22, where three different flows are indicated via the choice of an appropriate β . The computed solutions, shown in figure 23, correspond to a supercritical β and are in response to either smooth, (2.20), or nonsmooth, (2.19), initial data.

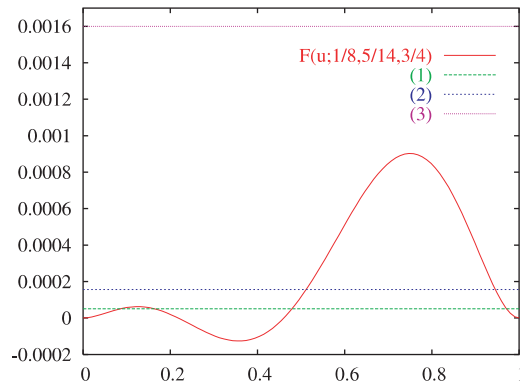


Figure 18. Graph of $F(u; 1/8, 5/14, 3/4)$. The horizontal lines of $1/\beta^2$ (1) ($\beta = 140$), (2) ($\beta = 80$) and (3) ($\beta = 25$) represent the supercritical, the intermediate and the subcritical regimes, respectively. Here, the local maxima are $F(u = 1/8) = 1/\beta_{*,2}^2 \approx 1/126.687^2$ and $F(u = 3/4) = 1/\beta_{*,1}^2 \approx 1/33.2881^2$.

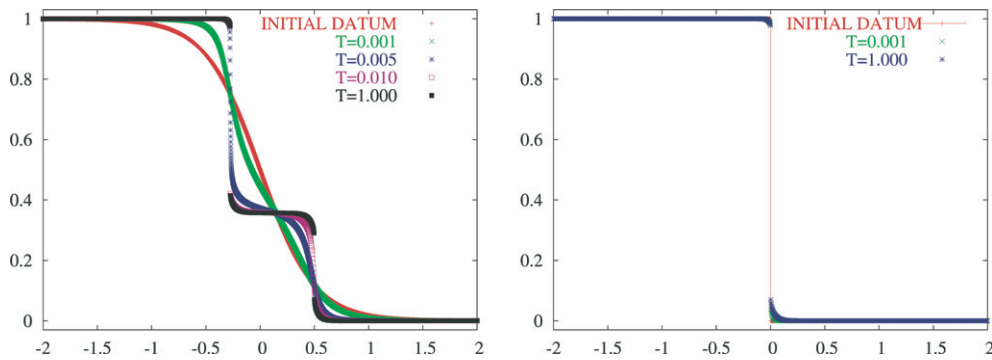


Figure 19. Solutions of (1.1), (1.3) with $f = f_5$ and the initial data (2.20) (left) and (2.19) (right). A supercritical $\beta = 140$; $\alpha_1 = 1/8, \alpha_2 = 5/14, \alpha_3 = 3/4$.

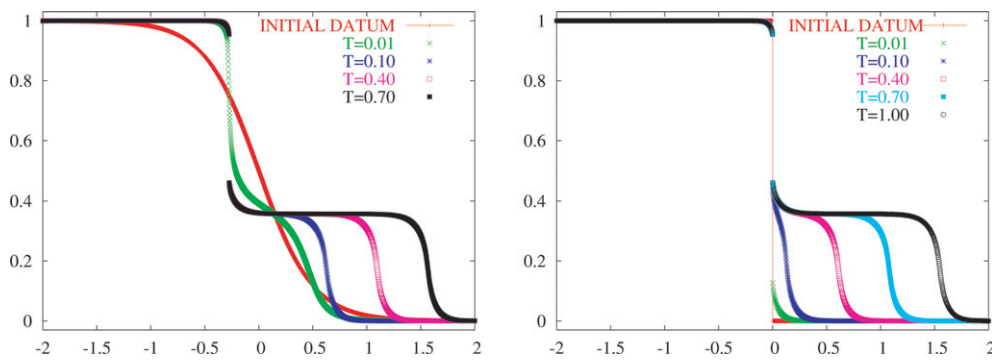


Figure 20. As in the previous figure, but with an intermediate $\beta = 80$.

3.2. The unbalanced case

The balanced case clearly indicates that both single and double jump structures are possible. The same conclusion can be also made in the unbalanced case. Here, as well as in the

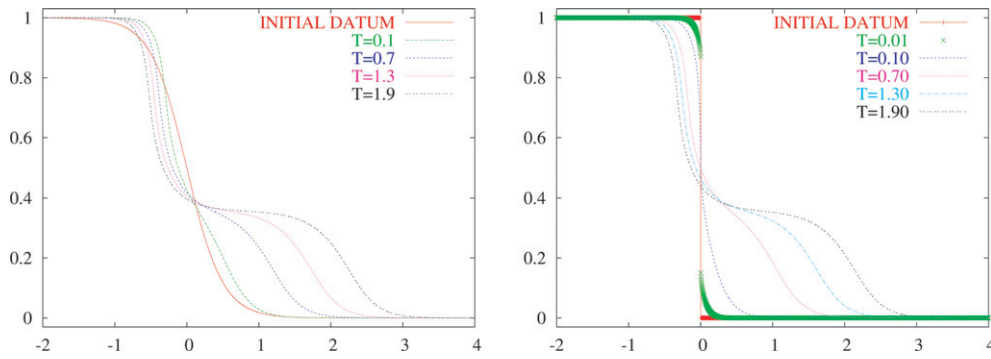


Figure 21. As in the previous two figures, but with a subcritical $\beta = 25$.

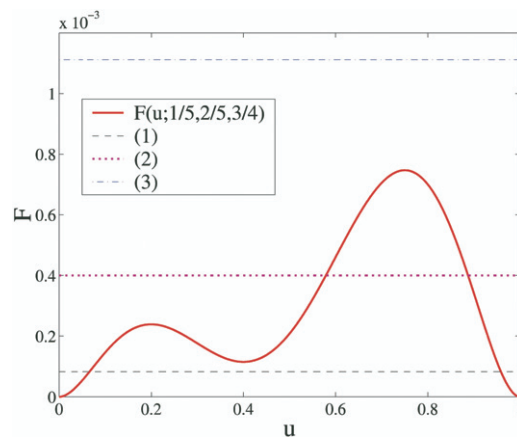


Figure 22. Graph of $F(u; 1/5, 2/5, 3/4)$. The horizontal lines of $1/\beta^2$ (1) ($\beta = 110$), (2) ($\beta = 50$) and (3) ($\beta = 30$) represent the supercritical, the intermediate and the subcritical regimes, respectively. Here, the local maxima are: $F(u = 1/5) = 1/\beta_{*,2}^2 \approx 1/64.6936^2$ and $F(u = 3/4) = 1/\beta_{*,1}^2 \approx 1/36.5864^2$.

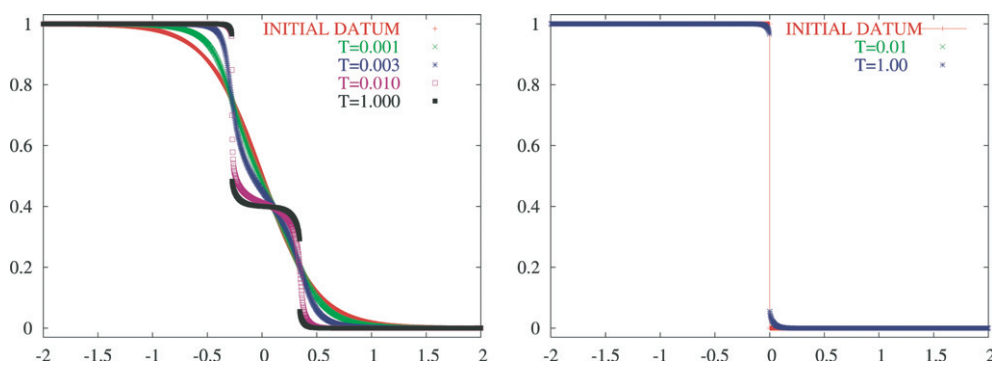


Figure 23. Solutions of (1.1), (1.3) with $f = f_5$ and the initial data (2.20) (left) and (2.19) (right). A supercritical $\beta = 110$; $\alpha_1 = 1/5, \alpha_2 = 2/5, \alpha_3 = 3/4$.

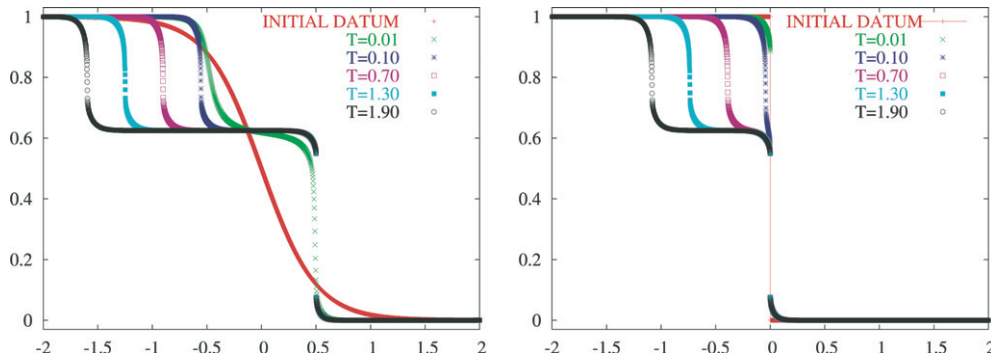


Figure 24. Solutions of (1.1), (1.3) with $f = f_5$ and the initial data (2.20) (left) and (2.19) (right). An intermediate $\beta = 95$; $\alpha_1 = 1/8$, $\alpha_2 = 3/8$, $\alpha_3 = 7/8$.

asymmetric balanced case, asymmetry of F implies that the two humps will, in general, be different implying shocks of different strength. Actually, in the quintic case the sharp distinction between balanced and unbalanced cases is blurred. Of course, in the subcritical unbalanced case we cannot obtain a conventional equilibrium, but otherwise the structure of F determines the outcome. As an example of that proximity compare the pattern in figure 24, wherein $\alpha_1 = 1/8$, $\alpha_2 = 5/8$, $\alpha_3 = 7/8$ and $\beta = 95$, with that of example 3, shown in figure 20. In spite of the fact that in the present example F is unbalanced, the pattern seems oblivious to this fact. Observe that β is subcritical with respect to one part of the flow and supercritical with respect to the other one. We note in passing one notable difference between the balanced and unbalanced cases: it concerns the way shock jumps are calculated. In the balanced case, figure 12 summarizes the strategy of balanced heating and cooling zones. In the unbalanced case, things are a bit more complex: one uses the fact that F being a primitive of f is defined up to a constant, which may be different for different smooth parts of the solution. Using the freedom to choose this constant enables one to determine the corresponding jump values in the unbalanced case.

3.3. Concluding comments

The quintic case, which even in the conventional case has a much richer morphology than the cubic one, supports an even richer morphology in the presence of saturating diffusion. It is not difficult to envision that as the reaction function becomes even more complicated the variety of solutions becomes very large. One point worth commenting upon is the robustness of the solutions in the supercritical and intermediate regimes. This was clearly demonstrated numerically; however, theoretically things are still very much in limbo for we were not able to provide for any of the attractors a rigorous mathematical proof. We have seen that in given supercritical conditions, depending on the choice of initial conditions we may obtain either one or two jumps. However, while the one-shock solution is clearly evolutionary, its robustness is limited. Since its emergence occurs only in an initial set-up with a large jump which, due to saturation of diffusion, freezes the spatial dynamics, large perturbation close enough to the front may destroy its one-jump pattern.

In order to demonstrate this, we consider the same equation as in example 1, but with the initial datum being a perturbation of the sharp jump (2.19):

$$u_0(x) = \begin{cases} 1, & \text{if } x < -0.5, \\ 1 + \varepsilon \sin(4\pi x), & \text{if } -0.5 < x < 0, \\ 0, & \text{if } x > 0. \end{cases} \quad (3.11)$$

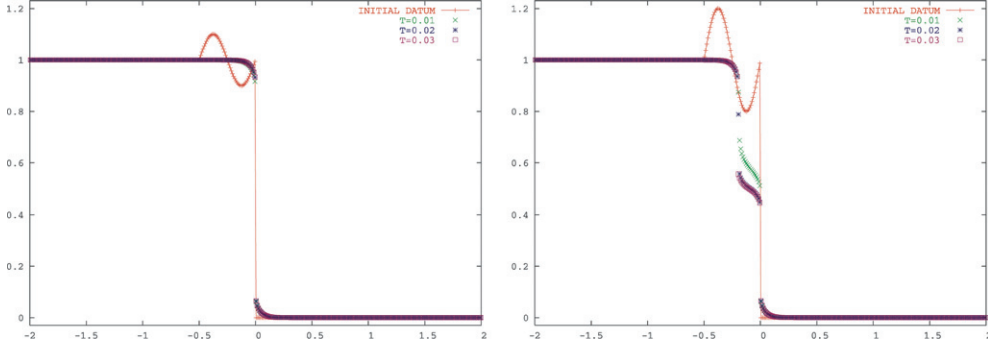


Figure 25. Solutions of (1.1), (1.3) with $f = f_5$ and the initial datum (3.11) with $\varepsilon = 0.1$ (left) and $\varepsilon = 0.2$ (right). A supercritical $\beta = 100$; $\alpha_1 = 1/8$, $\alpha_2 = 1/2$, $\alpha_3 = 7/8$.

The numerical results with $\varepsilon = 0.1$ and $\varepsilon = 0.2$ are shown in figure 25. As one can clearly see there, the small perturbation ($\varepsilon = 0.1$) is absorbed, while the large one ($\varepsilon = 0.2$) breaks the sharp front and instead the two-shock solution emerges. In general, the distance between the shocks depends on the amplitude, the width and the specific form of the perturbation.

4. A two-dimensional extension

This brief section is intended to exemplify the impact of saturated diffusion on reaction-diffusion processes in the plane. To this end, we consider the following equation:

$$u_t = Q(u_x, u_y)_x + R(u_x, u_y)_y - \beta^2 f(u), \quad (4.1)$$

where, as in the 1D case, f is a smooth function, for example, given by (1.4), and Q and R are smooth bounded functions, satisfying the condition of (weak) parabolicity (see, e.g. [10]). Typical diffusion fluxes, which have been used in our numerical experiments, are

$$Q(u_x, u_y) = \frac{u_x}{\sqrt{1 + u_x^2 + u_y^2}}, \quad R(u_x, u_y) = \frac{u_y}{\sqrt{1 + u_x^2 + u_y^2}}. \quad (4.2)$$

Equations (4.1) and (4.2), and (1.4) are solved over the rectangle $[-2.5, 2.5] \times [-1.5, 1.5]$ subject to the Neumann boundary condition and the following initial data:

$$u(x, y, 0) = \begin{cases} 1, & \text{if } (x, y) \in \mathcal{S}, \\ 0, & \text{otherwise,} \end{cases} \quad (4.3)$$

where the set $\mathcal{S} = \{(x, y) \mid (x, y) \in [-\frac{3}{2}, -\frac{1}{2}] \times [-\frac{1}{2}, \frac{1}{2}] \cup [-\frac{1}{2}, \frac{1}{2}] \times [-\frac{1}{20}, \frac{1}{20}] \cup [\frac{1}{2}, \frac{3}{2}] \times [-\frac{1}{2}, \frac{1}{2}]\}$. The numerical solutions, computed for $\beta = 10$ and $\beta = 30$ at times $t = 0.5$ and $t = 2$, are presented in figures 26 and 27. For comparison purposes, in figure 28, we show the numerical solutions for the same initial-value problems, but with the linear $Q(u_x, u_y) = u_x$ and $R(u_x, u_y) = u_y$ (note that the results are shown at time $t = 0.5$ only since by time $t = 2$, the numerical solutions for both $\beta = 10$ and $\beta = 30$ will almost converge to constant steady states).

One clearly observes the dramatic impact that saturation has on the diffusive spread and the consequential patterns.

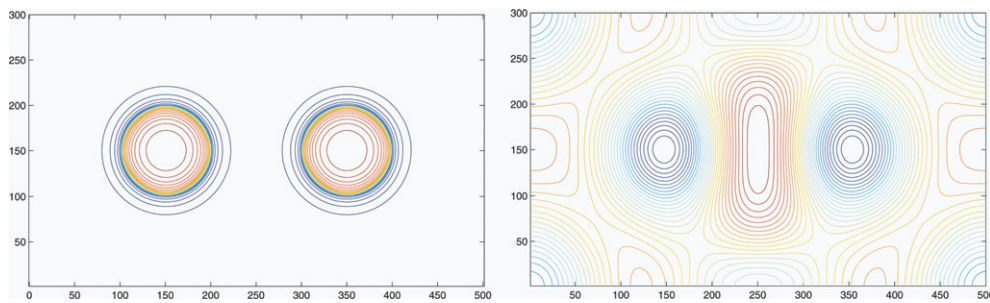


Figure 26. Saturating Q . $\beta = 10$. $t = 0.5$ (left) and $t = 2$ (right).

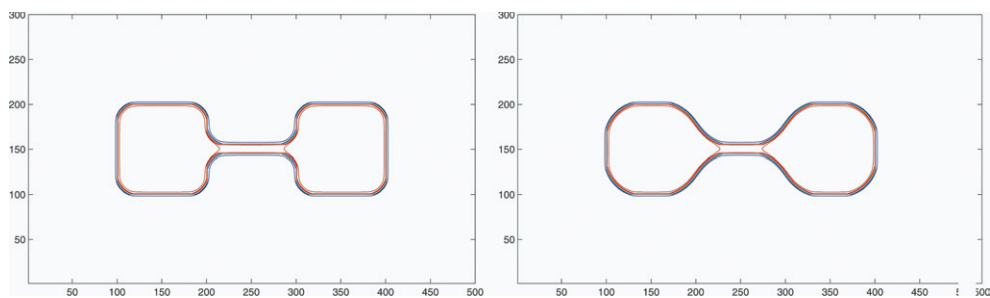


Figure 27. Saturating Q . $\beta = 30$. $t = 0.5$ (left) and $t = 2$ (right).

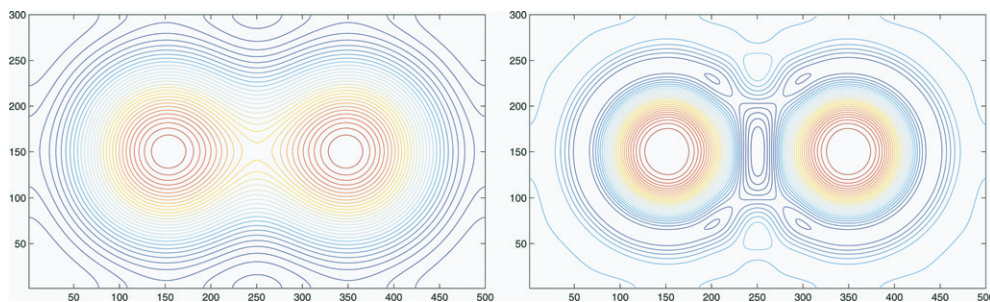


Figure 28. Linear Q . $\beta = 10$ (left) and $\beta = 30$ (right). $t = 0.5$.

Acknowledgments

The work of AK was supported in part by the NSF Grant #DMS-0310585. The research of PR was supported in part by the Israel Science Foundation Contract #558/99-2 and was done in part during his visit to the CNLS/T7 Theory Groups in the summer of 2004.

References

- [1] Bates P W, Fife P C, Ren W and Wang X 1997 Traveling waves in a convolution model for phase transitions *Arch. Rat. Mech. Anal.* **138** 105–36
- [2] Bertsch M and Dal Passo R 1992 Hyperbolic phenomena in a strongly degenerate parabolic equation *Arch. Rat. Mech. Anal.* **117** 1–32

- [3] Chertock A, Kurganov A and Rosenau P 2003 Formation of discontinuities in flux-saturated degenerate parabolic equations *Nonlinearity* **16** 1875–98
- [4] Chertock A, Kurganov A and Rosenau P 2005 On degenerate saturated-diffusion equations with convection *Nonlinearity* **18** 609–30
- [5] Erneux T and Nicolis G 1993 Propagating waves in discrete bistable reaction–diffusion systems *Physica D* **67** 237–44
- [6] Fife P C and Wang X 1998 A convolution model for interfacial motion: the generation and propagation of internal layers in higher space dimensions *Adv. Diff. Eqns* **3** 85–110
- [7] Goodman J, Kurganov A and Rosenau P 1999 Breakdown in Burgers-type equations with saturating dissipation fluxes *Nonlinearity* **12** 247–68
- [8] Kladko K, Mitkov I and Bishop A R 2000 Universal scaling of wave propagation failure in arrays of coupled nonlinear cells *Phys. Rev. Lett.* **84** 4505–8
- [9] Kurganov A and Rosenau P 1997 Effects of a saturating dissipation in Burgers-type equations *Commun. Pure Appl. Math.* **50** 753–71
- [10] Ladyženskaja O A, Solonnikov V A and Ural’ceva N N 1967 Linear and quasilinear equations of parabolic type (*Trans. Math. Monographs* vol 23) (Providence, RI: American Mathematical Society)
- [11] Rosenau P 1992 Tempered diffusion: a transport process with propagating fronts and inertial delay *Phys. Rev. A* **46** 7371–4
- [12] Rosenau P Diffusion models with saturated diffusion, unpublished
- [13] Rosenau P 1990 Free energy functionals at the high gradient limit *Phys. Rev. A* **41** 2227–30
- [14] Rosenau P, Hagan P, Northcutt R and Cohen D 1989 Delayed diffusion due to flux limitation *Phys. Lett. A* **142** 26–30
- [15] Rykov Yu G 2000 Discontinuous solutions of some strongly degenerate parabolic equations *Russ. J. Math. Phys.* **7** 341–62
- [16] Wang X 2002 Metastability and stability of patterns in a convolution model for phase transitions *J. Diff. Eqns* **183** 434–61